Atomic Structure of 2 nm Size Metallic Cobalt Prepared by Electrochemical Conversion: An in Situ Pair Distribution Function Study

Wei Li, Olaf Borkiewicz, Matthieu Saubanère, Marie-Liesse Doublet, Delphine Flahaut, Peter Chupas, Karena W Chapman, Damien Dambournet

Atomic Structure of 2-nm Size Metallic Cobalt Prepared by Electrochemical Conversion: An *In* Situ Pair Distribution Function Study

Wei Li,[‡] *Olaf J. Borkiewicz,*[▽] *Matthieu Saubanère,*[#,Δ] *Marie-Liesse Doublet,*[#,Δ] *Delphine Flahaut,*[§,Δ] *Peter J. Chupas,*[▽] *Karena W. Chapman,*[▽] *Damien Dambournet.*[‡,Δ*]

[‡] Sorbonne Université, CNRS, Physico-chimie des électrolytes et nano-systèmes interfaciaux, PHENIX, F-75005 Paris, France

[▽] X-ray Science Division, Advanced Photon Source, Argonne National Laboratory, Argonne, Illinois 60439, USA

[#] Institut Charles Gerhardt, UMR 5253, CNRS - Université Montpellier, Place Eugène Bataillon, 34 095 Montpellier, France

[§] Université de Pau et des Pays de l'Adour, IPREM/ECP (UMR 5254), Hélioparc, 2 av. Pierre Angot, 64053 Pau Cedex 9, France

[Δ] Réseau sur le Stockage Electrochimique de l'Energie (RS2E), FR CNRS 3459, 80039 Amiens cedex, France

ABSTRACT. Conversion reactions, offering high capacity in batteries, imply a restructuration of the pristine atomic structure down to the nanoscale. The associated large broadening in the Bragg peaks of restructured electrode renders the description of atomic structure, almost impossible using conventional x-ray diffraction. On the other hand, atomic pair distribution function is well suited to probe the structure of few nanometer size particles. Here, we investigated the formation mechanism and structure of 2-nm particle size of metallic Co obtained by electrochemical conversion of CoF_2. We found that the conversion process stabilized a disordered structure consisting of an *hcp-fcc* intergrowth. The reaction was followed by in-situ PDF providing unique insight into the growth of highly defective Co nanoparticles.

INTRODUCTION

Metallic cobalt displays numerous properties in the field of catalysis, magnetism and biomedicine that largely depend on the size/shape and structural features.[1–3] The latter point is not trivial as metallic Co presents several polymorphs including the face-centered-pack (*fcc*) and hexagonal-close-pack (*hcp*) arrangements which have close formation energies, *i.e.*, *hcp* is only 20 meV more stable than *fcc*.[4] Both polymorphs are structurally related, built from a close-packing of atoms and differing from the stacking sequence of this common plane, *i.e.*, the stacking sequences ABA and ABC produce the *hcp* and *fcc* crystal structures **(Figure S1)**, respectively. Downsizing the particle size can lead to the *hcp-fcc* intergrowth resulting in a disordered structure featuring stacking faults.[5] Typically, such a disordered structure arises from the fact that the two layers A-B can be followed by either C (to form *fcc* structure) or A (*hcp* structure). The level of stacking faults can be quantified by a probability of stacking faults. For

example, a 50% probability of stacking faults implies that there is an equal proportion of *hcp* and *fcc* sequences, a situation referring to a randomly stacked layers.[6]

As a technological relevant material, significant works were performed to describe the atomic structure of Co nanoparticles including the simulation of X-ray diffraction powder pattern by the Debbye equation,[5,6] ^{59}Co solid-state NMR,[7] and X-ray absorption spectroscopy[5,8,9].

Solving the atomic structure of disordered and ultra-small particles was called the "nanostructure problem".[10] The reason is that both finite size and disorder effects contribute to the loss of long-range order, which precludes the use of conventional x-ray diffraction. The pair distribution function (PDF) obtained by Fourier Transform of the so-called correlation function,[11] represents the probability of finding a pair of atoms separated from a distance *r*. The pair distribution function technique as total scattering analysis can probe the short to long-range order and can therefore be used whatever the crystalline state of the material. It is, therefore, one of the most suited technique to study the atomic structure of ultra-small objects.[12–14]

Solution-based synthesis has been largely used to control the size and shape of metallic Co nanoparticles.[15,16] Another approach that allows synthetizing ultra-small, *i.e.*, < 5 nm, and monodisperse nanoparticles relies on alkaline-ion driven electrochemical conversion.[17] In such reactions, a multi-electron process occurs leading to the reduction of the transition metal to form metal M^0 and lithiated nano-composite according to: $M^{z+}X_y + zLi^+ + ze^- \leftrightarrow M^0 + yLi_{z/y}X$, where X comprised O, N, S, P, F, and H.[17–21] One of the particularity of this process is the disintegration of the parent particle upon reduction, leading to ultra-small M/LiX composite with typical metallic cluster sizes ranging from 1 to 3 nm.[18] During the formation of the metal nanoparticles, their structure evolves and adapts to the close environment which is related to interfaces with LiX and MX and the passivating film arising from the electrolyte decomposition

and MX/LiX.[13,22] Much progresses have been made toward the fundamental understanding of the conversion-based mechanisms.[22–28] Moreover, these reactions provide also unique opportunities to design ultra-small objects with unique structural and physico-chemical properties.[29]

In the present work, we investigated the lithium electrochemical conversion reaction occurring in CoF_2, a potential high capacity electrode. We undertook to investigate the atomic structure of metallic cobalt formed upon Li-driven electrochemical reaction. By using *in*-situ pair distribution function, we concluded on the formation of 2-nm size of Co featuring *hcp-fcc* intergrowth. Our study further supports the suitability of the PDF method to solve complex nanostructure and provides novel insight into the complexity of conversion reactions.

RESULTS and DISCUSSION

The electrochemical reduction of CoF_2 *vs.* Li^+/Li is characterized by a single plateau region typical of a phase transition as observed for conversion processes **(Figure 1)**. A voltage plateau at 1.2 V leads to a capacity of *ca.* 800 mAh/g. According to the conversion reaction: $CoF_2 + 2Li = Co^0 + 2\ LiF$, the theoretical capacity is 553 mAh g^{-1} which indicates the completion of the reaction along with extra capacities arising from the decomposition of the electrolyte **(Figure S2)**. During the charge process, a plateau region is observed at *ca.* 3 V highlighting voltage hysteresis in agreement with literature data.[30] Moreover, the reaction is not completely reversible as the charge capacity reaches around 400 mAh g^{-1}, equivalent to 1.5 exchanged electrons.

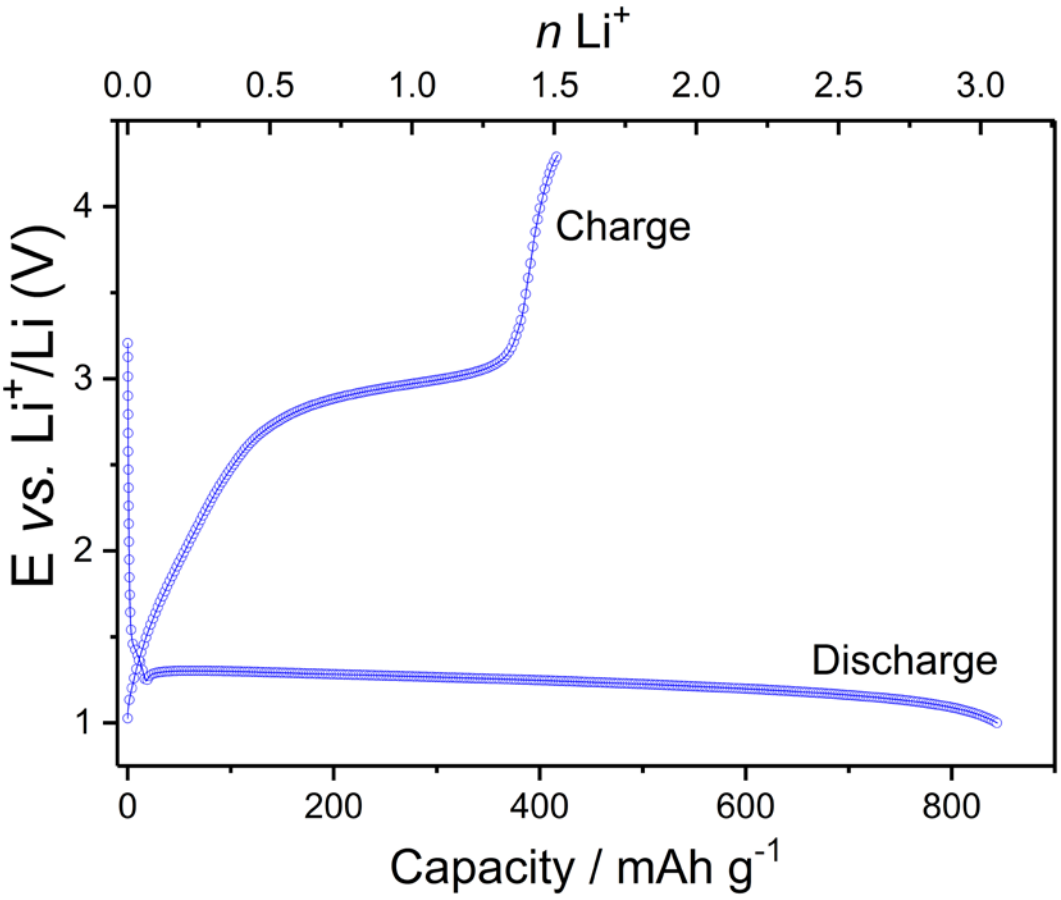

Figure 1. Galvanostatic discharge-charge curves of CoF_2 *vs.* Li^+/Li. Cells were cycled under 27.74 $mA.g^{-1}$ within 1-4.3 V voltage range. The curves correspond to the ones recorded during the *in*-situ PDF measurement.

High-resolution transmission electron microscopy was performed on a fully reduced CoF_2 electrode. **Figure 2** shows TEM images before and after the discharge. It reveals that the conversion process induces the pulverization of the pristine CoF_2 particles into *ca.* 2 nm size of metal cobalt characterized by a darker image contrast. Lattice fringes indicated that the particles are crystallized. Moreover, the particles appear agglomerated but not interconnected as found in metallic Fe formed by electrochemical conversion of FeF_2.[31] Fast Fourier Transformation (FFT) was performed on a large number of nanoparticles. The analysis revealed inter-reticular distances

that are characteristics of both *hcp* and *fcc* polymorphs (**Table S1**). Although both polymorphs feature close inter-reticular distances, we clearly distinguished both polymorphs signatures with distances at *ca.* 1.92 Å characteristic of the (101) plane of the *hcp* structure **(Figure 2, inset)**, and at *ca.* 1.8 Å characteristic of the (200) plane of the *fcc* structure. The smallest size of the particles, however, prevents to discern whether these particles are made of *hcp-fcc* intergrowth or physical mixture.

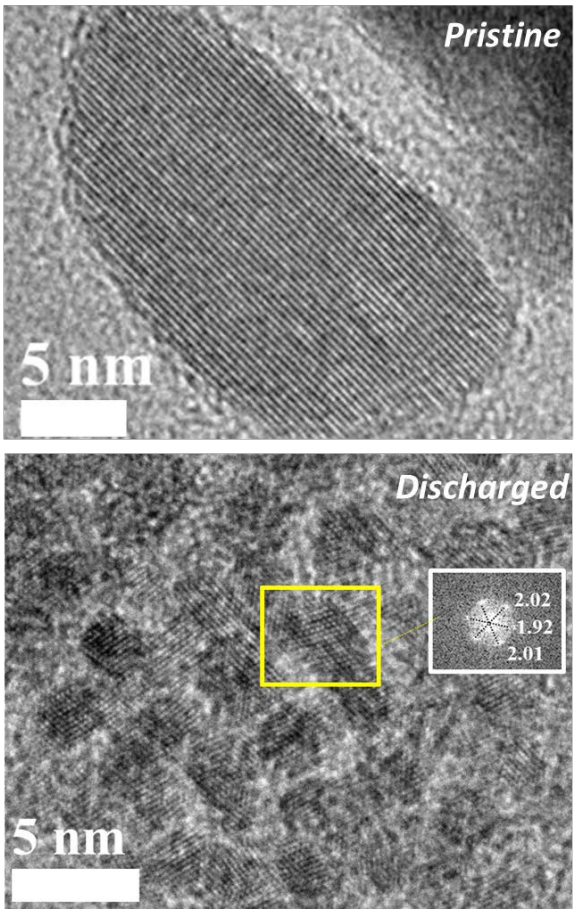

Figure 2. TEM images of the pristine CoF_2 and the CoF_2 electrode discharged to 1 V.

To capture the real atomic changes occurring during the electrochemical reaction, we turned to in-situ experiments.[32–34] We used *in*-situ high energy X-rays (λ = 0.2128 Å) data obtained with the AMPIX (Argonne's Multi-Purpose In situ X-ray) electrochemical cell (see experimental

section).[35] The typical x-ray diffraction powder pattern of a fully discharged electrode is shown in **Figure 3**. For the sake of clarity, the data were re-scaled in two-theta at the wavelength of copper λ_{Cu}=1.54 Å. Besides the expected Bragg peaks of LiF phase, we observed broad peaks belonging to metallic cobalt. The significant peak broadening is typical of ultra-small nanoparticles. Moreover, *hcp-fcc* intergrowth can also contribute to the Bragg peaks broadening.[6] Based on this pattern, it is again difficult to distinct whether the stabilized phase is made of *hcp-fcc* intergrowth or physical mixture. A broad peak located at ca. 51.5° (2θ), however, allows to identify the presence of the *fcc* form. The presence of the *hcp* signature observed by TEM, however, cannot be clearly identified on this XRD pattern.

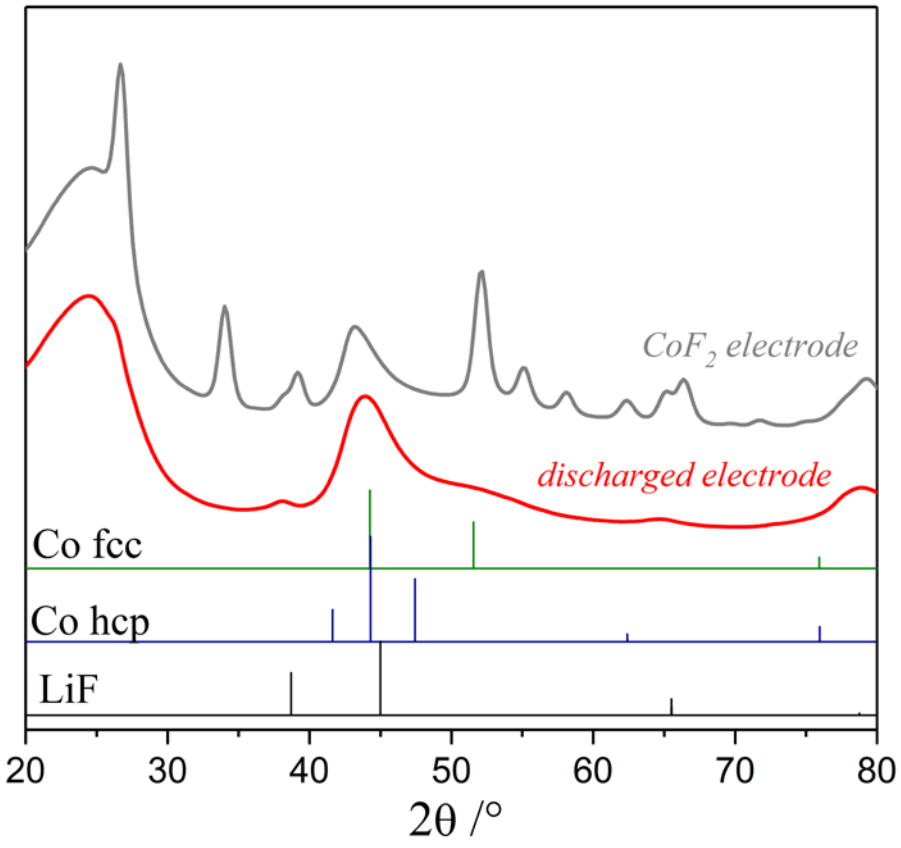

Figure 3. X-ray diffraction patterns of CoF_2 electrode before and after the first discharge. The schematic x-ray diffraction patterns of LiF, *hcp* and *fcc* are presented.

As the recorded x-ray data contain both the Bragg and diffuse components, we turned to the pair distribution function to get more insight into the atomic structure of metallic Co formed during the electrochemical conversion of CoF_2. Selected PDFs taken during the electrochemical discharge and charge processes were plotted in **Figure 4**. The low *r*-region shows the progressive nucleation growth of metallic Co at the expense of CoF_2. The peak located at ca. 2.05 Å from Co-F pairs progressively disappears while metallic Co-Co pairs appear at *ca.* 2.5 Å as found in *fcc* and *hcp* polymorphs. The completion of the conversion reaction can be further evidenced by the disappearance of the peak located at 3.67 Å corresponding to Co-Co distances in CoF_2.

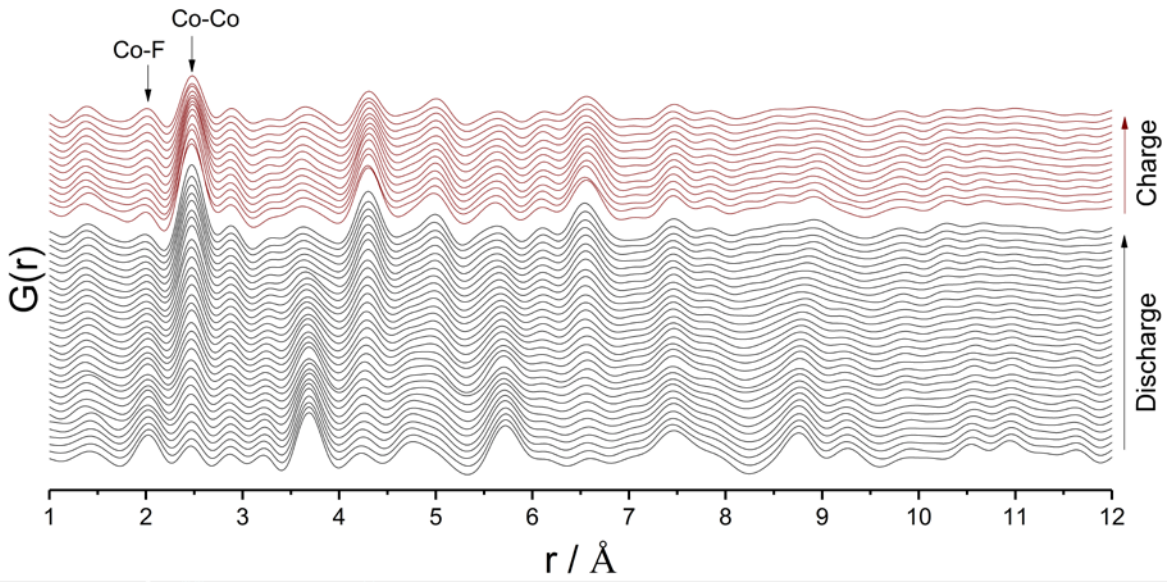

Figure 4. Selected PDFs of cycled CoF_2 electrode *vs.* Li^+/Li.

To further support the description of the atomic structure of metallic Co prepared by electrochemical reaction, a principal component analysis (PCA) of the operando PDF data were undertaken to assess the number of independently varying components involved in the reaction.[36] This multivariable statistical method allows to treat a large set of volume data without any prior consideration of structural models. The scree plot that represents the fraction of total variance

(Figure S3) indicates that there are only two significant components. The two main components along with their weighting during the discharge reaction are shown in **Figure 5**. The first component includes features related to the CoF_2 precursor and has a decreasing contribution during the reaction. The second component includes features related to metallic Co and increases in contribution during the reaction. The absence of a significant third component ruled out the formation of a mixture of *hcp* and *fcc* phases, suggesting the formation of *hcp-fcc* intergrowth.

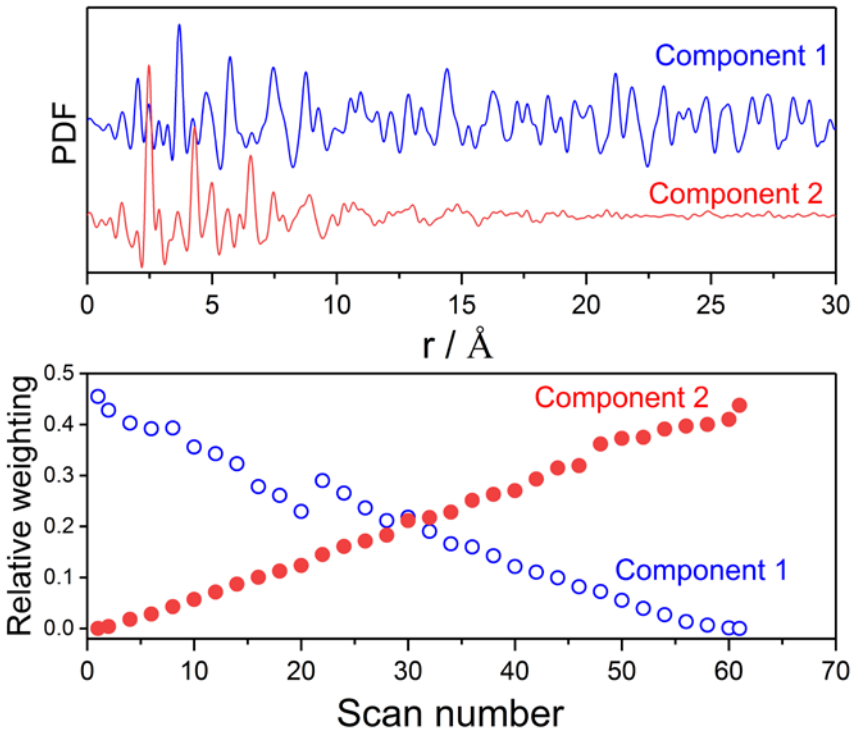

Figure 5. The first two components obtained by the PCA analysis of PDF data obtained during the discharge reaction. The component 1 includes features of the precursor CoF_2 and component 2 was identified as metallic Co.

To understand the atomic structure of electrochemically formed metallic Co, we first attempt to refine the PDF data after completion of the discharge process **(Figure 5)**. Using the *hcp* structure does not lead to a satisfying refinement, *i.e.*, R_w = 36.4 %. The quality of the fit significantly improved when modelling the PDF with the *fcc* polymorph (R_w = 24.4 %). In the difference

curve, however, a peak located at 4.8 Å is not captured by the model. This peak is characteristic of Co-Co distance found in the ABA sequence of *hcp* structure **(Figures S1,S4)** which further attests for the formation of *hcp-fcc* intergrowth. The accurate description of stacking faulted structure implies to build model systems that can be refined over the experimental data using programs such as Discus, FAULTS or DIFFAX.[37–39] Another approach to describe the stacking faulted structure consists of using a mixed-phase model.[40] Although this method is less accurate, it is less time-consuming and was shown to be suited for nanoparticles size of 2-nm.[40] Using the mixed-phase model, the final refinement was good with a further improvement of the fit to R_w = 19.3 % **(Figure 5)**. The refined parameter values were gathered in **Table 1**. The quantitative phase analysis showed a slightly larger proportion of the *fcc* phase which seems to agree with literature suggesting that the *fcc* structure is more stable than the *hcp* for small particles.[41] Moreover, the refined unit cell parameter of the *fcc* phase was a = 3.538 Å, a value close to that reported for bulk *fcc*.[42] The lattice parameters of the *hcp* phase, however, are strikingly different from the bulk values (a = 2.506 Å and c = 4.069 Å), particularly along the *c*-axis.[42,43] This might be due to a slightly larger interlayer in the *fcc* stacking as compared to *hcp* stacking. Hence, the presence of *hcp* stacking should have a slightly larger interlayer to match those of the *fcc* structure. Finally, the refined scattering domain was around 2-nm which is in good agreement with the particle sizes observed by TEM.

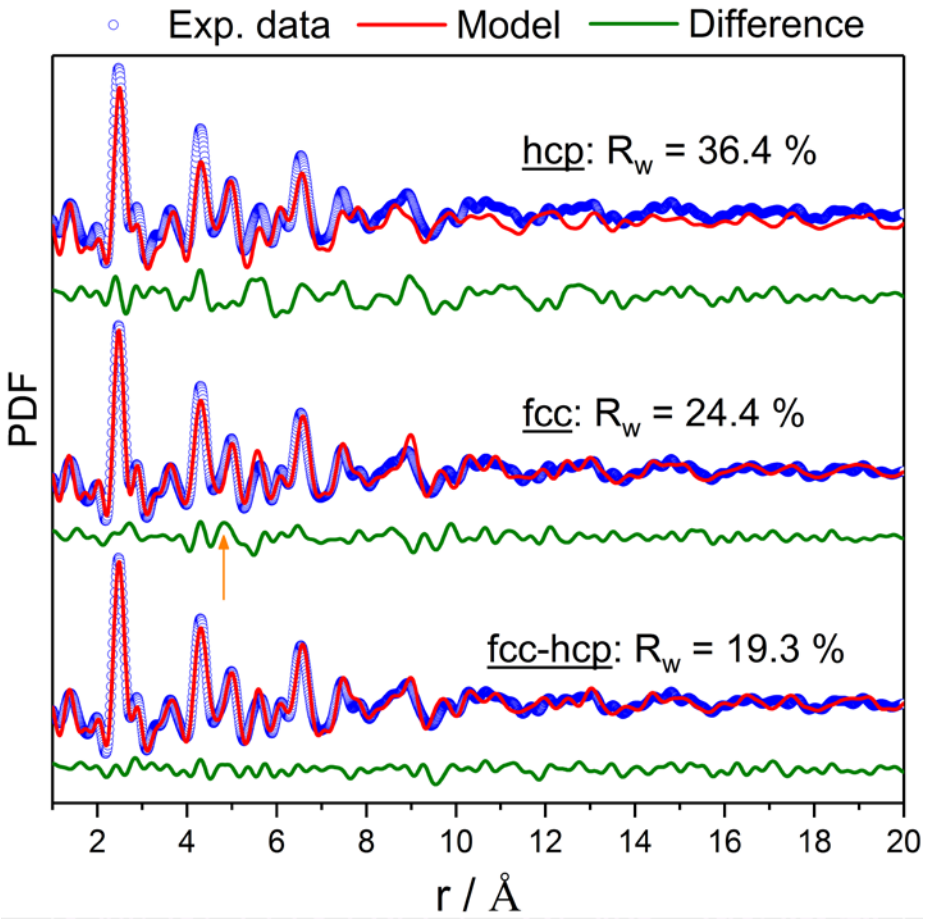

Figure 5. Fits to the experimental PDFs with *hcp*, *fcc* and *fcc-hcp* models. The orange arrow indicates the Co-Co distance found in the ABC stacking of the *hcp* polymorph.

Table 1. Refined parameter values obtained from PDF refinement of the fully discharged electrode using a mixed-phase modelling to account for *hcp-fcc* intergrowth.

	fcc	**hcp**
Unit cell parameters (Å)	a = 3.538(1)	a = 2.478(2) c = 4.186(9)
Relative phase content (%)	56.4	43.6
Co ADP (Å^2)	0.0093(1)	
spdiameter (Å)	20.5(3)	

To monitor structural changes occurring during electrochemical reactions, we refined the PDF data recorded during the first cycle. Upon discharge, the analysis shows the progressive conversion of CoF_2 into metallic Co occurring within the plateau region **(Figure 7)**. We note that the unit cell parameters of CoF_2 did not vary upon reduction suggesting the absence of any insertion reaction prior to the conversion process **(Figure S5)**. We used the mixed-phase modelling to detect the formation of disordered structure made of *hcp-fcc* intergrowth along the course of the discharge reaction. The results showed the phase's content remains constant during the discharge reaction suggesting that disordered nanoparticles made of *hcp-fcc* intergrowth are continuously generated by the electrochemical reduction of CoF_2. This is good agreement with the PCA that revealed only one Co-based conversion product. We note that the estimated standard deviation obtained on the metallic Co phase fractions decreases as the reaction progresses. Moreover, we monitored the changes in the unit cell parameters of the two-phase **(Figure S6)** with similar unit cell parameters for both phases.

Upon charge, the voltage plateau located at 3 V was associated with the reformation of CoF_2 as confirmed by PDF refinement **(Figure 7, Figure S7)**. Similarly, to other conversion-based electrodes, the re-oxidized phase features short-range ordering (denoted as amorphous) with a scattering domain of 14 Å. At the end of the charge, the ratio between the *fcc* and *hcp* remains almost constant again supporting the mechanism based on the stabilization of nanoparticles made of *hcp-fcc* intergrowth.

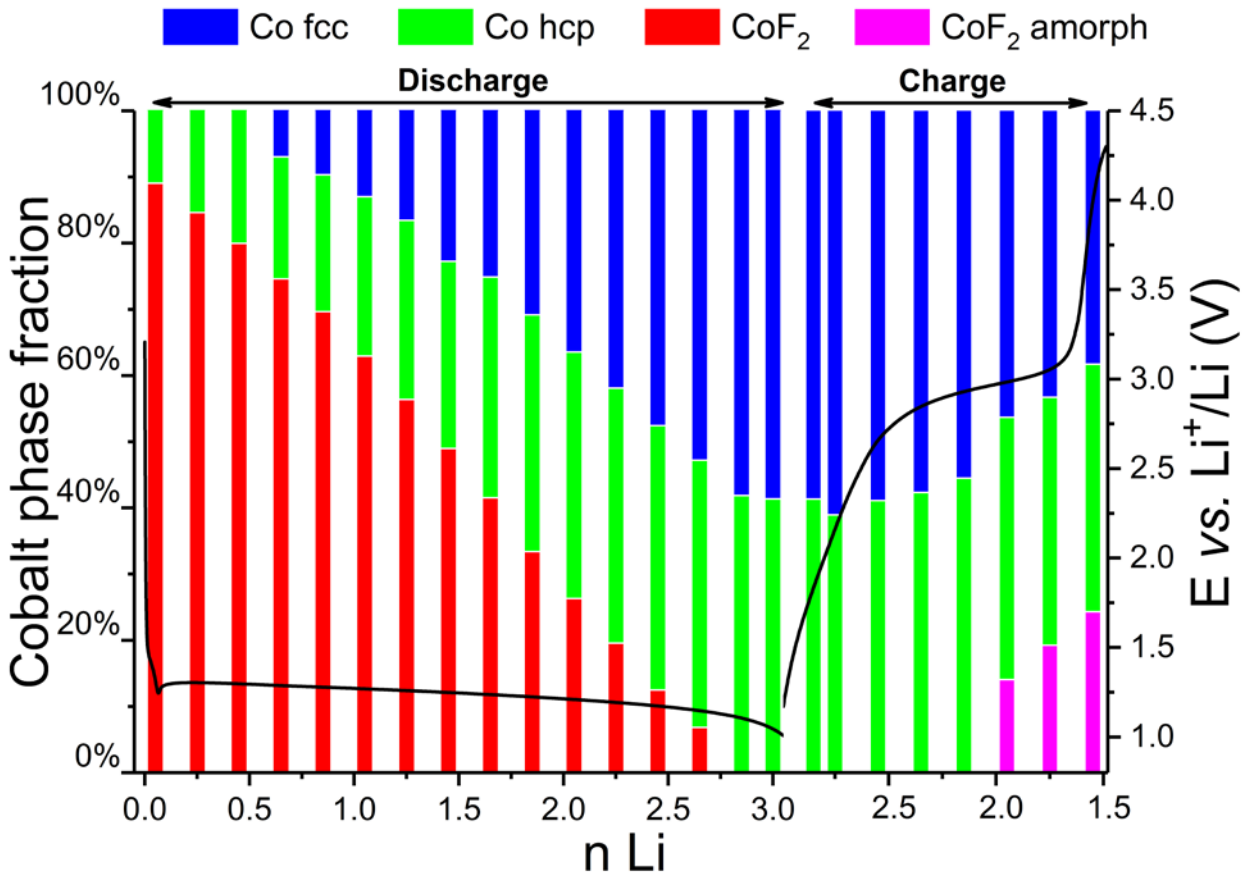

Figure 7. Quantitative phase analysis obtained by PDF refinements during the first cycle.

CONCLUSION

In summary, we investigated the structural evolution of CoF_2 during the Li-driven electrochemical conversion by means of *in*-situ PDF method. We found that CoF_2 is converted to 2-nm size metallic cobalt whose atomic structure consists of nanoparticles made of *hcp-fcc* intergrowth. Upon charging, a highly disordered CoF_2 phase is formed back proving the reversibility of the reaction. This study provides unique insights into the atomic structural description of conversion-based products and shows that efforts on understanding conversion processes should be pursued to fully describe these complex reactions and enabled practical applications.

EXPERIMENTAL SECTION

PDF analysis. For in-situ PDF analysis, electrodes were made by mixing active material CoF_2 (51 wt%), carbon ("super P", Alfa Aesar), carbon black and PTFE binder (Sigma-Aldrich) into pellet with total mass of 21.7 mg, 10 mm diameter and 120-180 μm thickness. Electrode pellet, fiber separator (Whatman GF/A), electrolyte (1 M $LiPF_6$ in 3:7 v:v ethylene carbonate: dimethylcarbonate (EC:DMC) from Tomiyama Pure Chemical Industries) and lithium foil as counter electrode were assembled into the AMPIX[35] electrochemical cell under Ar atmosphere in a glovebox. Cell was cycled galvanostatically against lithium at a C/20 rate (27.74 mA/g) within the voltage window 1-4.3 V (see Figure 1). X-ray total scattering data were collected every 30 min.

X-ray total scattering data were collected at the 11-ID-B beamline at the Advanced Photon Source, Argonne National Laboratory, using high energy X-rays (λ = 0.2128 Å) to high values of momentum transfer Q_{max} = 18 $Å^{-1}$.[44,45] The raw total scattering data were integrated in Fit2D.[46] PDFs, G(r) were obtained by Fourier transform after eliminating Kapton and background contributions within PDFgetX2.[47]

The refinement of the PDF data was performed using PDFgui.[48] The Q_{damp} was fixed to 0.04. The structural models used were CoF_2, graphite (to account for the large amount of carbon within the electrode), LiF, Co *hcp*, Co *fcc*. The refined parameters includes lattice parameters, scale factor, *s*ratio (*i.e.* low-*r* to high-*r* PDF peak ratio correction due to the correlated motion of bonded atoms[49]), spdiameter (*i.e.* particle diameter), and isotropic atomic displacement factors (ADPs). For the two-phase refinement including *fcc* and *hcp* structural models, ADP for Co, sratio and spdiameter were refined and constrained to an identical value for both polymorphs. The phase fraction obtained for the

fully discharged electrode gave 25 wt.% of metallic Co, 28 wt.% of LiF and 46 wt.% of carbon. These proportions are close to those expected based on the electrode composition and completion of the conversion reaction. The purity of the pristine CoF_2 was confirmed by PDF refinement (Figure S8).

The quality of the refinement is quantified by the reliability factor weighted R-value, denoted as R_w. The R-value describes the difference between the experimental observation (data) and the calculated value (fit) for a single data point. The R_w is the R-value weighted for data point *i*, and is given by the formula:

$$R_w = \sqrt{\frac{\sum_{i=1}^{N} w(r_i)[G_{obs}(r_i) - G_{calc}(r_i)]^2}{\sum_{i=1}^{N} w(r_i) G_{obs}^2(r_i)}}$$

with G_{obs} and G_{calc} being the observed (data) and calculated (fit) PDF and $w(r_i)$ the weight for each data point.

TEM analysis. To perform TEM analysis, coin cells were disassembled in a glove box. The discharged electrodes were washed with DMC to remove $LiPF_6$ and EC. After evaporating DMC, the electrodes were analyzed by TEM using a JEOL 2010 UHR microscope operating at 200 kV equipped with a TCD camera.

X-ray Photoelectron Spectroscopy (XPS). XPS analyses were performed on a Kratos Axis Ultra spectrometer with a focused monochromatized Al Kα radiation (1486.6 eV). The analysis chamber was in a $5x10^{-9}$ mbar vacuum. The applied current was 10 mA and the voltage 10 kV. The spectrometer pass energy was set to 20 eV to record the core peaks. The size of the excitation beam was 700x400 μm^2. Surface charging was minimized using a neutralizer gun which sprays low energy electrons over the sample surface. The samples were prepared in a glove box under Ar and transferred to the XPS analyzer under a controlled atmosphere to prevent

any surface contamination with ambient atmosphere. The samples were fixed on the sample holder with a Cu double tape. All the binding energy (B.E.) scale was calibrated from the adventitious carbon C 1s peak set at 285.0 eV. We performed at least three analyses for each sample. The quantification of atoms for surface composition was based on Scofield's relative sensitivity factors.[50]

ASSOCIATED CONTENT

Supporting Information. XPS analysis, crystallographic data of Co *hcp* and Co *fcc*, structural parameters obtained from PDF refinement, scree plot, PDF refinement of the charged electrode. This material is available free of charge via the Internet at http://pubs.acs.org.

AUTHOR INFORMATION

Corresponding Author

* damien.dambournet@sorbonne-universite.fr

ACKNOWLEDGMENT

This research used resources of the Advanced Photon Source, a U.S. Department of Energy (DOE) Office of Science User Facility operated for the DOE Office of Science by Argonne National Laboratory under Contract No. DE-AC02-06CH11357. We thanks A. Demourgues and C. Pepin for providing CoF_2 samples and S. Casale for TEM analysis. D.D thanks the French network on fluorine chemistry (GIS-FLUOR) for support.

REFERENCES

(1) Price, S. W. T.; Martin, D. J.; Parsons, A. D.; Sławiński, W. A.; Vamvakeros, A.; Keylock, S. J.; Beale, A. M.; Mosselmans, J. F. W. Chemical Imaging of Fischer-Tropsch

Catalysts under Operating Conditions. *Sci. Adv.* **2017**, *3* (3).

(2) Chakroune, N.; Viau, G.; Ricolleau, C.; Fiévet-Vincent, F.; Fiévet, F. Cobalt-Based Anisotropic Particles Prepared by the Polyol Process. *J. Mater. Chem.* **2003**, *13* (2), 312–318.

(3) Jun, Y.; Seo, J.; Cheon, J. Nanoscaling Laws of Magnetic Nanoparticles and Their Applicabilities in Biomedical Sciences. *Acc. Chem. Res.* **2008**, *41* (2), 179–189.

(4) Jain, A.; Ong, S. P.; Hautier, G.; Chen, W.; Richards, W. D.; Dacek, S.; Cholia, S.; Gunter, D.; Skinner, D.; Ceder, G.; et al. Commentary: The Materials Project: A Materials Genome Approach to Accelerating Materials Innovation. *APL Mater.* **2013**, *1* (1), 011002.

(5) Longo, A.; Sciortino, L.; Giannici, F.; Martorana, A. Crossing the Boundary between Face-Centred Cubic and Hexagonal Close Packed: The Structure of Nanosized Cobalt Is Unraveled by a Model Accounting for Shape, Size Distribution and Stacking Faults, Allowing Simulation of XRD, XANES and EXAFS. *J. Appl. Crystallogr.* **2014**, *47* (5), 1562–1568.

(6) Sławiński, W. A.; Zacharaki, E.; Fjellvåg, H.; Sjåstad, A. O. Structural Arrangement in Close-Packed Cobalt Polytypes. *Cryst. Growth Des.* **2018**, *18* (4), 2316–2325.

(7) Speight, R.; Wong, A.; Ellis, P.; Bishop, P. T.; Hyde, T. I.; Bastow, T. J.; Smith, M. E. $^{59}\text{C}\text{o}$ NMR Study of the Allotropic Phase Transformation in Small Ferromagnetic Cobalt Particles. *Phys. Rev. B* **2009**, *79* (5), 054102.

(8) Sprouster, D. J.; Giulian, R.; Schnohr, C. S.; Araujo, L. L.; Kluth, P.; Byrne, A. P.; Foran, G. J.; Johannessen, B.; Ridgway, M. C. Fcc-Hcp Phase Transformation in Co Nanoparticles Induced by Swift Heavy-Ion Irradiation. *Phys. Rev. B* **2009**, *80* (11), 115438.

(9) Sciortino, L.; Giannici, F.; Martorana, A.; Ruggirello, A. M.; Liveri, V. T.; Portale, G.; Casaletto, M. P.; Longo, A. Structural Characterization of Surfactant-Coated Bimetallic Cobalt/Nickel Nanoclusters by XPS, EXAFS, WAXS, and SAXS. *J. Phys. Chem. C* **2011**, *115* (14), 6360–6366.

(10) Billinge, S. J. L.; Levin, I. The Problem with Determining Atomic Structure at the Nanoscale. *Science* **2007**, *316* (5824), 561–565.

(11) Keen, D. A. A Comparison of Various Commonly Used Correlation Functions for Describing Total Scattering. *J. Appl. Crystallogr.* **2001**, *34* (2), 172–177.

(12) Masadeh, A. S.; Božin, E. S.; Farrow, C. L.; Paglia, G.; Juhas, P.; Billinge, S. J. L.; Karkamkar, A.; Kanatzidis, M. G. Quantitative Size-Dependent Structure and Strain Determination of CdSe Nanoparticles Using Atomic Pair Distribution Function Analysis.

Phys. Rev. B **2007**, *76* (11), 115413.

(13) Shyam, B.; Chapman, K. W.; Balasubramanian, M.; Klingler, R. J.; Srajer, G.; Chupas, P. J. Structural and Mechanistic Revelations on an Iron Conversion Reaction from Pair Distribution Function Analysis. *Angew. Chem. Int. Ed.* **2012**, *51* (20), 4852–4855.

(14) Jensen, K. M. Ø.; Juhas, P.; Tofanelli, M. A.; Heinecke, C. L.; Vaughan, G.; Ackerson, C. J.; Billinge, S. J. L. Polymorphism in Magic-Sized $Au_{144}(SR)_{60}$ Clusters. *Nat. Commun.* **2016**, *7*, 11859.

(15) Puntes, V. F.; Krishnan, K. M.; Alivisatos, A. P. Colloidal Nanocrystal Shape and Size Control: The Case of Cobalt. *Science* **2001**, *291* (5511), 2115–2117.

(16) Lu, A.-H.; Salabas, E. L.; Schüth, F. Magnetic Nanoparticles: Synthesis, Protection, Functionalization, and Application. *Angew. Chem. Int. Ed. 46* (8), 1222–1244.

(17) Poizot, P.; Laruelle, S.; Grugeon, S.; Dupont, L.; Tarascon, J.-M. Nano-Sized Transition-Metal Oxides as Negative-Electrode Materials for Lithium-Ion Batteries. *Nature* **2000**, *407* (6803), 496–499.

(18) Cabana, J.; Monconduit, L.; Larcher, D.; Palacín, M. R. Beyond Intercalation-Based Li-Ion Batteries: The State of the Art and Challenges of Electrode Materials Reacting Through Conversion Reactions. *Adv. Mater.* **2010**, *22* (35), E170–E192.

(19) Li, H.; Richter, G.; Maier, J. Reversible Formation and Decomposition of LiF Clusters Using Transition Metal Fluorides as Precursors and Their Application in Rechargeable Li Batteries. *Adv. Mater.* **2003**, *15* (9), 736–739.

(20) Badway, F.; Cosandey, F.; Pereira, N.; Amatucci, G. G. Carbon Metal Fluoride Nanocomposites High-Capacity Reversible Metal Fluoride Conversion Materials as Rechargeable Positive Electrodes for Li Batteries. *J. Electrochem. Soc.* **2003**, *150* (10), A1318–A1327.

(21) Oumellal, Y.; Rougier, A.; Nazri, G. A.; Tarascon, J.-M.; Aymard, L. Metal Hydrides for Lithium-Ion Batteries. *Nat. Mater.* **2008**, *7* (11), 916–921.

(22) Dalverny, A.-L.; Filhol, J.-S.; Doublet, M.-L. Interface Electrochemistry in Conversion Materials for Li-Ion Batteries. *J. Mater. Chem.* **2011**, *21* (27), 10134–10142.

(23) Wang, F.; Yu, H.-C.; Chen, M.-H.; Wu, L.; Pereira, N.; Thornton, K.; Ven, A. V. der; Zhu, Y.; Amatucci, G. G.; Graetz, J. Tracking Lithium Transport and Electrochemical Reactions in Nanoparticles. *Nat. Commun.* **2012**, *3*, 1201.

(24) Hu, Y.-Y.; Liu, Z.; Nam, K.-W.; Borkiewicz, O. J.; Cheng, J.; Hua, X.; Dunstan, M. T.; Yu, X.; Wiaderek, K. M.; Du, L.-S.; et al. Origin of Additional Capacities in Metal Oxide

Lithium-Ion Battery Electrodes. *Nat. Mater.* **2013**, *12* (12), 1130–1136.

(25) Abraham, A.; Housel, L. M.; Lininger, C. N.; Bock, D. C.; Jou, J.; Wang, F.; West, A. C.; Marschilok, A. C.; Takeuchi, K. J.; Takeuchi, E. S. Investigating the Complex Chemistry of Functional Energy Storage Systems: The Need for an Integrative, Multiscale (Molecular to Mesoscale) Perspective. *ACS Cent. Sci.* **2016**, *2* (6), 380–387.

(26) Wiaderek, K. M.; Borkiewicz, O. J.; Castillo-Martínez, E.; Robert, R.; Pereira, N.; Amatucci, G. G.; Grey, C. P.; Chupas, P. J.; Chapman, K. W. Comprehensive Insights into the Structural and Chemical Changes in Mixed-Anion FeOF Electrodes by Using Operando PDF and NMR Spectroscopy. *J. Am. Chem. Soc.* **2013**, *135* (10), 4070–4078.

(27) Wiaderek, K. M.; Borkiewicz, O. J.; Pereira, N.; Ilavsky, J.; Amatucci, G. G.; Chupas, P. J.; Chapman, K. W. Mesoscale Effects in Electrochemical Conversion: Coupling of Chemistry to Atomic- and Nanoscale Structure in Iron-Based Electrodes. *J. Am. Chem. Soc.* **2014**, *136* (17), 6211–6214.

(28) Ma, Y.; Garofalini, S. H. Atomistic Insights into the Conversion Reaction in Iron Fluoride: A Dynamically Adaptive Force Field Approach. *J. Am. Chem. Soc.* **2012**, *134* (19), 8205–8211.

(29) Hu, Y.-S.; Guo, Y.-G.; Sigle, W.; Hore, S.; Balaya, P.; Maier, J. Electrochemical Lithiation Synthesis of Nanoporous Materials with Superior Catalytic and Capacitive Activity. *Nat. Mater.* **2006**, *5* (9), 713–717.

(30) Teng, Y. T.; Pramana, S. S.; Ding, J.; Wu, T.; Yazami, R. Investigation of the Conversion Mechanism of Nanosized CoF2. *Electrochimica Acta* **2013**, *107*, 301–312.

(31) Wang, F.; Robert, R.; Chernova, N. A.; Pereira, N.; Omenya, F.; Badway, F.; Hua, X.; Ruotolo, M.; Zhang, R.; Wu, L.; et al. Conversion Reaction Mechanisms in Lithium Ion Batteries: Study of the Binary Metal Fluoride Electrodes https://pubs.acs.org/doi/abs/10.1021/ja206268a (accessed May 25, 2018).

(32) Luo, L.; Wu, J.; Xu, J.; Dravid, V. P. Atomic Resolution Study of Reversible Conversion Reaction in Metal Oxide Electrodes for Lithium-Ion Battery. *ACS Nano* **2014**, *8* (11), 11560–11566.

(33) Chapman, K. W. Emerging Operando and X-Ray Pair Distribution Function Methods for Energy Materials Development. *MRS Bull.* **2016**, *41* (03), 231–240.

(34) Yu, S.-H.; Feng, X.; Zhang, N.; Seok, J.; Abruña, H. D. Understanding Conversion-Type Electrodes for Lithium Rechargeable Batteries. *Acc. Chem. Res.* **2018**, *51* (2), 273–281.

(35) Borkiewicz, O. J.; Shyam, B.; Wiaderek, K. M.; Kurtz, C.; Chupas, P. J.; Chapman, K. W. The AMPIX Electrochemical Cell: A Versatile Apparatus for in Situ X-Ray Scattering and

Spectroscopic Measurements. *J. Appl. Crystallogr.* **2012**, *45* (6), 1261–1269.

(36) Chapman, K. W.; Lapidus, S. H.; Chupas, P. J. Applications of Principal Component Analysis to Pair Distribution Function Data. *J. Appl. Crystallogr.* **2015**, *48* (6), 1619–1626.

(37) Proffen, T.; Neder, R. B. DISCUS: A Program for Diffuse Scattering and Defect-Structure Simulation. *J. Appl. Crystallogr.* **1997**, *30* (2), 171–175.

(38) Casas-Cabanas, M.; Reynaud, M.; Rikarte, J.; Horbach, P.; Rodríguez-Carvajal, J. FAULTS: A Program for Refinement of Structures with Extended Defects. *J. Appl. Crystallogr.* **2016**, *49* (6), 2259–2269.

(39) Treacy, M. M. J.; Newsam, J. M.; Deem, M. W. A General Recursion Method for Calculating Diffracted Intensities from Crystals Containing Planar Faults. *Proc. Math. Phys. Sci.* **1991**, *433* (1889), 499–520.

(40) Yang, X.; Masadeh, A. S.; McBride, J. R.; Božin, E. S.; Rosenthal, S. J.; Billinge, S. J. L. Confirmation of Disordered Structure of Ultrasmall CdSe Nanoparticles from X-Ray Atomic Pair Distribution Function Analysis. *Phys. Chem. Chem. Phys.* **2013**, *15* (22), 8480–8486.

(41) Kitakami, O.; Sato, H.; Shimada, Y.; Sato, F.; Tanaka, M. Size Effect on the Crystal Phase of Cobalt Fine Particles. *Phys. Rev. B* **1997**, *56* (21), 13849–13854.

(42) Owen, E. A.; Jones, D. M. Effect of Grain Size on the Crystal Structure of Cobalt. *Proc. Phys. Soc. Sect. B* **1954**, *67* (6), 456.

(43) Feygenson, M.; Formo, E. V.; Freeman, K.; Schieber, N.; Gai, Z.; Rondinone, A. J. Implications of Room Temperature Oxidation on Crystal Structure and Exchange Bias Effect in Co/CoO Nanoparticles. *J. Phys. Chem. C* **2015**, *119* (46), 26219–26228.

(44) Chupas, P. J.; Qiu, X.; Hanson, J. C.; Lee, P. L.; Grey, C. P.; Billinge, S. J. L. Rapid-Acquisition Pair Distribution Function (RA-PDF) Analysis. *J. Appl. Crystallogr.* **2003**, *36* (6), 1342–1347.

(45) Chupas, P. J.; Chapman, K. W.; Lee, P. L. Applications of an Amorphous Silicon-Based Area Detector for High-Resolution, High-Sensitivity and Fast Time-Resolved Pair Distribution Function Measurements. *J. Appl. Crystallogr.* **2007**, *40* (3), 463–470.

(46) Hammersley, A. P.; Svensson, S. O.; Hanfland, M.; Fitch, A. N.; Hausermann, D. Two-Dimensional Detector Software: From Real Detector to Idealised Image or Two-Theta Scan. *High Press. Res.* **1996**, *14* (4-6), 235–248.

(47) Qiu, X.; Thompson, J. W.; Billinge, S. J. L. PDFgetX2: A GUI-Driven Program to Obtain the Pair Distribution Function from X-Ray Powder Diffraction Data. *J. Appl. Crystallogr.*

2004, *37* (4), 678–678.

(48) Farrow, C. L.; Juhas, P.; Liu, J. W.; Bryndin, D.; Božin, E. S.; Bloch, J.; Proffen, T.; Billinge, S. J. L. PDFfit2 and PDFgui: Computer Programs for Studying Nanostructure in Crystals. *J. Phys. Condens. Matter* **2007**, *19* (33), 335219.

(49) Egami, T.; Billinge, S. J. L. *Underneath the Bragg Peaks: Structural Analysis of Complex Materials*; Elsevier, 2003.

(50) Scofield, J. H. Hartree-Slater Subshell Photoionization Cross-Sections at 1254 and 1487 eV. *J. Electron Spectrosc. Relat. Phenom.* **1976**, *8* (2), 129–137.

TOC Graphic